

# Direct Method of Hydraulic Conductivity Structure Identification for Subsurface Transport Modeling

Jianyong Jiao<sup>1</sup> and Ye Zhang<sup>2</sup>

**Abstract:** Solute transport in aquifers is strongly influenced by the spatial distribution of subsurface hydraulic conductivity ( $K$ ), while limited drilling typically results in lack of data characterizing both the  $K$  and the in situ fluid-flow boundary conditions (BC). To characterize such environments, this paper presents an efficient direct inverse method to simultaneously identify an aquifer's  $K$  pattern, values, and flow field. The method ensures fluid-flow continuity using local approximate solutions of the governing flow equation conditioned to limited measurements, while the physics of flow are enforced, making the inverse problem well-posed. A single system of equations is assembled and solved, from which parameters and BC can be simultaneously estimated. For problems with irregular and regular  $K$  distributions, inversion is demonstrated for different measurement types, qualities, and quantities. When measurement error is increased, the estimated  $K$  pattern is largely insensitive to the error, although the inverted flow field suffers greater inaccuracy. Local conductivity and Darcy flux measurements are found to have similar information content, although subtle differences exist in the inversion outcomes when long-term contaminant release is simulated. Local conductivity measurements lead to better identification of conductivity pattern, values, and hydraulic head field; Darcy flux measurements lead to more-accurate estimation of the velocity field and thus improved transport predictions. Overall, velocity field estimated by the direct inverse method based on hydraulic measurements can lead to reasonable predictions of contaminant migration under unknown aquifer BC. DOI: 10.1061/(ASCE)HE.1943-5584.0001410. © 2016 American Society of Civil Engineers.

**Author keywords:** Inverse method; Aquifer; Parameter structure identification; Contaminant transport.

## Introduction

Transport processes in aquifers are critically controlled by hydraulic head gradient, porosity, and the spatial distribution of hydraulic conductivity ( $K$ ). In environmental and energy studies, the heterogeneity patterns of aquifer  $K$  exert a first-order impact on fluid-flow pathways and where/when solute transport and breakthrough occur. Accordingly, subsurface flow and transport models have become increasingly elaborate, and it is common to create complex two-dimensional and three-dimensional grids to represent spatial heterogeneity, which then enables detailed delineation of the solute transport pathways. Limited spatial borehole data for subsurface environments, however, generally lead to a poor knowledge of  $K$  heterogeneity and therefore to significant uncertainty in both flow and transport predictions using models. As the subsurface is increasingly used both as a resource (e.g., water, hydrocarbon, geothermal extraction) and energy and waste repository (e.g., natural gas storage, geologic CO<sub>2</sub> sequestration, and waste disposal), subsurface characterization has received significant attention in recent years. In both shallow and deep aquifers, however, whenever borehole access is limited, subsurface fluid-flow boundary conditions (including both the Dirichlet and the Neuman boundaries) are highly uncertain in addition to the uncertain distribution of conductivity. Clearly, aquifer characterization requires the estimation

of both  $K$  distribution and the in situ fluid-flow boundary conditions (BC), which together determine the aquifer state, i.e., hydraulic head and fluid velocity. Velocity, in particular, determines pathways and rates of solute transport.

To estimate conductivity, direct measurement via aquifer-stimulation techniques often suffer the well-known scale effect that occurs as  $K$  measurements depend on the volume being tested (Sanchez-Vila et al. 1996; Zlotnik et al. 2000; Zhang et al. 2007). Thus,  $K$  values measured at smaller support volumes may not adequately represent the values at greater grid-cell volumes. By developing a numerical model,  $K$  values of the model can be calibrated with inverse methods based on measurements of the hydrological state variables, e.g., water levels, flow rates, and solute concentrations (Hill and Tiedeman 2007). This article presents a computationally efficient direct inverse method that uses hydraulic measurements to simultaneously estimate  $K$  patterns, values, and flow fields, including the unknown aquifer BC. By reconstructing the velocity distribution, contaminant transport in the aquifer can then be predicted. The next paragraphs will briefly review prior research on parameter identification. The next sections will then illustrate the direct method in greater detail.

Sun and Yeh (1985) and Carrera and Neuman (1986b) were among the first to propose parameter structure identification in aquifer inversion. Subsequently, different methods were developed, including the Pilot Points method, Sequential Self-Calibration, Moment Equations Method, Representer Method, Zonation Method, and Semianalytical Method, among others. The Pilot Points method was first proposed by de Marsily (1978), its key feature consisting of kriging the parameter values at pilot points and measurement locations (if they exist) to create the parameter field during inversion (Certes and de Marsily 1991; Alcolea et al. 2006b, a). The sequential self-calibration method (Gomez-Hernandez et al. 1997) was the first to create multiple equally-likely stochastic realizations, providing unbiased estimates of hydraulic heads and concentrations. The

<sup>1</sup>Postdoctoral Fellow, Dept. of Geology and Geophysics, Univ. of Wyoming, Laramie, WY 82071 (corresponding author). E-mail: jjiao1@uwo.edu

<sup>2</sup>Associate Professor, Dept. of Geology and Geophysics, Univ. of Wyoming, Laramie, WY 82071. E-mail: yzhang9@uwo.edu

Note. This manuscript was submitted on June 18, 2015; approved on March 14, 2016; published online on May 31, 2016. Discussion period open until October 31, 2016; separate discussions must be submitted for individual papers. This paper is part of the *Journal of Hydrologic Engineering*, © ASCE, ISSN 1084-0699.

moment equations method relies on a nonlinear geostatistical inverse algorithm (Hernandez et al. 2006), while the representer method is widely used in meteorological and oceanographic sciences (Kurapov et al. 2007, Ngodock et al. 2006) before it was adopted in hydrogeological investigation to estimate large-scale patterns of transmissivity and dispersivity from scattered measurements of head, concentration, and transmissivity (Bennet 1992; Pebesma and Wesseling 1998; Przybylski-Jarnut et al. 2007). The zonation method was developed by Carrera and Neuman (1986a, b), and due to its close link to the classic concept of hydrostratigraphy (or hydrofacies, petrofacies, flow units, lithofacies, and so on), has become widely adopted by practitioners. Stauffer et al. (2000) used the semianalytical method to assess uncertainty of the well catchments for pumping in heterogeneous aquifers. Most aquifer inverse methods, including the studies cited here, do not differ in their essential approaches, but only in their implementation or computational detail (Ginn and Cushman 1990; McLaughlin and Townley 1996; Carrera et al. 2005; Vrugi et al. 2008; Yeh et al. 1996; Lu and Robinson 2006; Dai and Samper 2004). A common scheme among them is the building and calibration of a forward simulation model with which model fit against field observations (i.e., model–data mismatch or objective function) is iteratively improved until model parameters and/or structures are identified. Because a forward model is needed, subsurface fluid flow (and transport) initial and boundary conditions are assumed known or are calibrated as part of the inverse solution. However, in deep aquifers, boundary conditions for fluid flow are rarely known. As demonstrated in Irsa and Zhang (2012), boundary condition calibration can lead to nonunique estimation of the parameters and flow field. Even when BC are reasonably known by drilling and sampling many wells or by conducting hydraulic tests near aquifer boundaries, errors in obtaining such information, similar to measurement errors, can lead to inaccurate inversion outcomes (Zhang et al. 2014). There is additionally the issue of study areas far from physical boundaries (e.g., river, fault, or aquifer pitch-out), for which fluid-flow BC needed for developing a site model are at best ambiguous and often unknown.

To address aquifer inversion under unknown BC, a computationally-efficient direct method is developed and proven accurate and robust for solving different fluid-flow inverse problems including those with significant source/sink effects (Irsa and Zhang 2012; Zhang 2014; Jiao and Zhang 2014b, a, 2015b, a). Boundary conditions were estimated from the results of inversion, while aquifer parameters were populated deterministically assuming that their patterns are known a priori. However, for data-poor and highly heterogeneous aquifers, both  $K$  patterns and BC are typically unknown. This work develops an improved approach to simultaneously estimate parameter structure, parameter values, and flow field (including the unknown BC), by adopting (1) local approximate solutions (LAS) of inversion, and (2) a suitable  $K$  parameterization that ensures the inverted  $K$  values are positive. The key improvement of this work thus lies in parameter structure identification. By inverting two synthetic aquifer problems with irregular versus regular facies distributions, inversion is demonstrated for different measurement types, qualities, and quantities. Transport simulation of long-term contaminant release into the aquifer is then carried out in the original and the reconstructed flow fields. Given the recovered velocity distribution, the contaminant pathway and breakthrough curves can then be accurately predicted.

## Method

The key difference between the direct method developed in this work and the majority of existing aquifer inversion techniques is

that an objective function based on model–data mismatch is not optimized, and therefore a forward groundwater model does not need to be built and simulated. An independent grid is developed for inversion and is referred to herein as the inversion grid. Aquifer hydraulic conductivity is assumed to follow the distribution of facies, whereas within-facies  $K$  is assumed uniform. However, unlike the zonation method (Carrera and Neuman 1986a, b; Jiao and Zhang 2014b), conductivity is formulated as a set of locally continuous functions with unknown coefficients that are mapped onto individual inversion grid cells. Inversion is then carried out in two steps: facies distribution is recovered first, followed by the estimation of their conductivities. The next section explains the inversion method in detail.

## Governing Flow Equation

The steady state two-dimensional (2D) groundwater flow equation for a confined aquifer without sources/sinks is

$$\frac{\partial}{\partial x} \left[ K(x, y) b \frac{\partial h(x, y)}{\partial x} \right] + \frac{\partial}{\partial y} \left[ K(x, y) b \frac{\partial h(x, y)}{\partial y} \right] = 0 \quad \text{on } \Omega \quad (1)$$

where  $h(x, y)$  = hydraulic head (L);  $K(x, y)$  = hydraulic conductivity (L/T);  $b$  = saturated thickness (assumed known); and  $\Omega$  = solution domain. To test inversion, Eq. (1) is solved in the forward mode by assigning a set of Dirichlet and no-flux BC to the domain boundaries. These BCs will be recovered in inversion along with the unknown parameters.

## Inverse Theory

For the steady-state flow problem described in Eq. (1), the inverse method for obtaining conductivity pattern enforces three sets of constraints: (1) global continuity of hydraulic head and Darcy fluxes at a set of collocation points (Fig. 1); (2) local conditioning of the inverse solutions to observed heads, fluxes, or locally

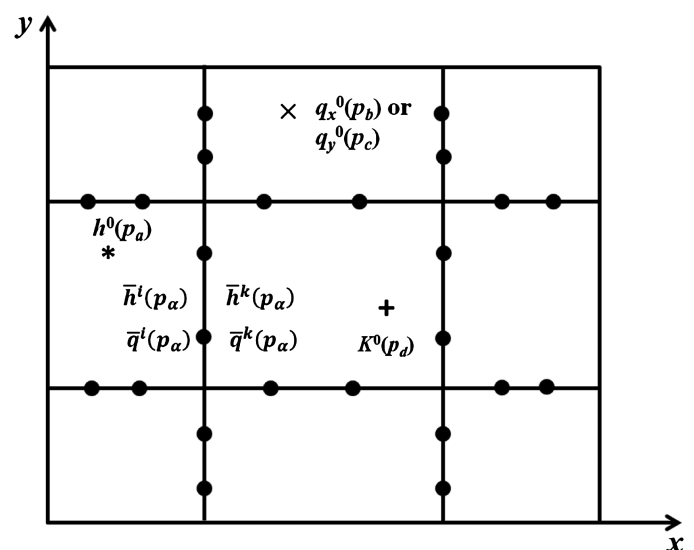


**Fig. 1.** Inversion grid discretization and a set of collocation points (filled circles); observed data for inversion are also shown: \* is observed head, + is observed local conductivity, and × is observed Darcy flux

observed hydraulic conductivities (Fig. 1); and (3) a set of equation constraints at selected points that enforces the flow physics.

The first set of constraints is written as

$$w(p_\alpha) \int R_h(p_\alpha) \delta(p_\alpha) d\Gamma_j = 0, \quad j = 1, \dots, Y; \quad \alpha = 1, \dots, V \quad (2)$$

$$w(p_\alpha) \int R_q(p_\alpha) \delta(p_\alpha) d\Gamma_j = 0, \quad j = 1, \dots, Y; \quad \alpha = 1, \dots, V \quad (3)$$

where  $p_\alpha$  = collocation point on the  $j$ th cell interface ( $\Gamma_j$ );  $\alpha$  = number of collocation points on  $\Gamma_j$ ;  $R_h(p_\alpha)$  and  $R_q(p_\alpha)$  = residuals of hydraulic head and Darcy fluxes at  $p_\alpha$  on  $\Gamma_j$ , respectively;  $Y$  = total number of cell interfaces in the inversion grid;  $\delta(p_\alpha)$  = Dirac delta function; and  $w(p_\alpha)$  = weighting function that samples the residuals at  $p_\alpha$  on  $\Gamma_j$ . The residuals can be expanded as

$$R_h(p_\alpha) = \bar{h}^i(p_\alpha) - \bar{h}^k(p_\alpha) \quad (4)$$

$$R_q(p_\alpha) = \bar{q}^i(p_\alpha) - \bar{q}^k(p_\alpha) \quad (5)$$

where  $\bar{h}$  and  $\bar{q}$  = set of proposed fundamental solutions of inversion; and  $i$  and  $k$  = cells in the inversion grid adjacent to  $\Gamma_j$ . For coordinate  $(x, y)$ ,  $\bar{q} = [q_x, q_y]$ . Because the fluid-flow pathway will refract at a facies interface whose location is unknown, it is problematic to impose continuity on both components of the  $\bar{q}$  vector at the collocation points, i.e.,  $\Gamma_j$  may coincide with a facies interface. To address this issue, continuity is enforced with one component only: if  $p_\alpha$  lies along  $\Gamma_j$  that is parallel to the  $x$  axis, continuity is enforced on  $q_y$ , and vice versa. This approach is found to work well for recognizing facies pattern using the orthogonal inversion grid of this study. Unlike Irsa and Zhang (2012) and Jiao and Zhang (2014b, a, 2015b) where the facies pattern is known prior to inversion and thus  $\Gamma_j$  honors the facies interface, the inversion grid here is independent of the facies pattern ( $\Gamma_j$  does not honor the facies interface), i.e., the same grid can be used for recognizing different facies patterns.

As the second set of constraints,  $\bar{h}$ ,  $\bar{q}$ , or hydraulic conductivity are conditioned at the measurement locations

$$w(p_a)[\bar{h}(p_a) - h^o(p_a)] = 0 \quad a = 1, \dots, A \quad (6)$$

$$w(p_b)[\bar{q}_x(p_b) - q_x^o(p_b)] = 0 \quad b = 1, \dots, B \quad (7)$$

$$w(p_c)[\bar{q}_y(p_c) - q_y^o(p_c)] = 0 \quad c = 1, \dots, C \quad (8)$$

$$w(p_d)[\bar{K}(p_d) - K^o(p_d)] = 0 \quad d = 1, \dots, D \quad (9)$$

where  $p_a$ ,  $p_b$ ,  $p_c$ , and  $p_d$  = measurement points;  $h^o$ ,  $q_x^o$ ,  $q_y^o$ , and  $K^o$  = observed heads, fluxes, and local conductivities at these points ( $A$ ,  $B$ ,  $C$ , and  $D$  are the total number of observations), respectively; and  $w(p_a)$ ,  $w(p_b)$ ,  $w(p_c)$ , and  $w(p_d)$  are weighting functions assigned to each observation equation to reflect the magnitude of the measurement errors. Inversion under both error-free and random measurement errors is investigated in this work. Either flux or  $K$  conditioning, or both, can lead to well-posed solutions (Zhang 2014). However, inversion cannot lead to unique  $K$  estimation by conditioning only to hydraulic head measurements. In this work, either flux or local  $K$  measurements are used, although inversion is also successful when both measurements are provided.

In this study, the fundamental solutions of inversion ( $\bar{h}$  and  $\bar{q}$ ) are local approximate solutions (LAS) rather than exact, as will be illustrated later. To enforce flow physics, a set of equation constraints is developed

$$w(p_e)R_e = \varepsilon \quad (10)$$

$$R_e = \left\{ \frac{\partial}{\partial x} \left[ Kb \frac{\partial h(x, y)}{\partial x} \right] + \frac{\partial}{\partial y} \left[ Kb \frac{\partial h(x, y)}{\partial y} \right] \right\} \Big|_e$$

$$e = 1, \dots, Y\alpha + A + B + C + D$$

where  $p_e$  includes both the collocation points and the head, flux, or local conductivity measurement locations; and  $R_e$  = residual of the governing flow equation at  $p_e$ . At these locations in the inversion grid, Eq. (10) enforces a set of physical flow constraints on the local solutions. The residual  $\varepsilon$  is set to be a small number rather than 0.0, e.g.,  $\varepsilon$  is less than  $10^{-4}$ .

## Facies Recognition

To create the LAS, a local flow equation is solved at each inversion grid cell ( $\Omega_e$ )

$$\frac{\partial}{\partial x} \left[ bK(x, y) \frac{\partial h(x, y)}{\partial x} \right] + \frac{\partial}{\partial y} \left[ bK(x, y) \frac{\partial h(x, y)}{\partial y} \right] = 0 \quad \text{on } \Omega_e \quad (11)$$

where Eq. (11) is discretized over  $\Omega$ ; and  $K(x, y)$  and  $b$  = local conductivity and saturated thickness of the grid cell, respectively. In this work, polynomial and exponential functions are proposed as the LAS of hydraulic head and conductivity, respectively

$$\bar{h}(x, y) = a_1 + a_2x + a_3y + a_4xy + a_5x^2 + a_6y^2 \quad \text{on } \Omega_e \quad (12)$$

$$\bar{K}(x, y) = \exp(a_7 + a_8x + a_9y + a_{10}xy) \quad \text{on } \Omega_e \quad (13)$$

where  $a_i$  ( $i = 1, \dots, 10$ ) = unknown cell-wise constants to be estimated by inversion. Using Darcy's law, Darcy flux can be approximated, also over  $\Omega_e$ , as

$$\bar{q}_x(x, y) = -\exp(a_7 + a_8x + a_9y + a_{10}xy)(a_2 + a_4y + 2a_5x) \quad (14)$$

$$\bar{q}_y(x, y) = -\exp(a_7 + a_8x + a_9y + a_{10}xy)(a_3 + a_4x + 2a_6y) \quad (15)$$

$\bar{h}(x, y)$  is any reasonable function that may approximate the behavior of flow locally, which may be obtained by examining the forward-flow solution. An exponential function is chosen to approximate the conductivity, which ensures that the estimated  $\bar{K}(x, y)$  is positive. The Darcy flux approximations are then derived from both functions.

To find the facies pattern, Eqs. (2)–(10) are first assembled, into which Eqs. (12)–(15) are substituted. The resulting system of nonlinear equations is solved (see "Solution Techniques"), with the solution of  $\mathbf{x}^T = [a_i^e]$ ,  $i = 1, \dots, 10$ ,  $e = 1, \dots, M$  (number of inversion grid cells). For each  $\Omega_e$ , then  $\bar{h}(x, y)$ ,  $\bar{K}(x, y)$ ,  $\bar{q}_x(x, y)$ , and  $\bar{q}_y(x, y)$  are reconstructed, from which both the Dirichlet and Neumann BC can be recovered along the domain boundaries. The facies pattern is then recognized by selecting an appropriate conductivity threshold ( $K_0$ ):  $K_0$  varies between  $K_1$  and  $K_2$  and is considered a form of prior information constraint for inversion. For a two-facies system, given a known  $K_0$  (generally

a value falling into 40–60th linear percentile between  $K_1$  and  $K_2$ ), the facies pattern is recovered by applying the following relation to the estimated  $\bar{K}(x, y)$  field:

$$\text{if } \bar{K}(x, y) < K_0, \quad (x, y) \in K_1 \text{ facies} \quad \text{if } \bar{K}(x, y) \geq K_0, \\ (x, y) \in K_2 \text{ facies} \quad (16)$$

As will be demonstrated later, Eq. (16) can be extended to  $m$  facies by selecting a set of  $(m - 1)$  threshold conductivities.

## Facies $K$ Estimation

To estimate the facies conductivities, Eqs. (2)–(10) are assembled and solved a second time, although a different set of LAS is used in inversion. At this point, the facies pattern has been derived and is assumed fixed. Using the same orthogonal grid as earlier, conductivity estimation is carried out via the new set of fundamental solutions, one for each inversion grid cell

$$\tilde{h}(x, y) = b_1 + b_2x + b_3y + b_4xy + b_5(x^2 - y^2) \quad \text{on } \Omega_e \quad (17)$$

$$\tilde{q}_x(x, y) = -K_v(b_2 + b_4y + 2b_5x) \quad (18)$$

$$\tilde{q}_y(x, y) = -K_v(a_3 + b_4x - 2b_5y) \quad (19)$$

where  $b_j$  ( $j = 1, \dots, 5$ ) is a new set of unknown coefficients of inversion, and

$$K_v = \begin{cases} K_1 & \text{if } (x, y) \in K_1 \text{ facies} \\ K_2 & \text{if } (x, y) \in K_2 \text{ facies} \end{cases}$$

To condition to the local conductivity measurements, Eq. (9) is given as

$$w(p_d)(K_v - K_i^o) = 0 \quad i = 1, D$$

where  $i$  = a location where an observed (noisy)  $K$  falls into a known facies type, although this facies type (inverted in the previous step) may suffer from classification errors. By substituting Eqs. (17)–(19) into Eqs. (2)–(10), a new system of inversion equations is established for which the solution is  $\mathbf{x}^T = [K_1, K_2, b_j^e]$ ,  $j = 1, \dots, 5$ ,  $e = 1, \dots, M$ . The same measurements used for facies identification are used for  $K$  estimation, and the preceding formulation can be extended to a number of facies whereby  $K_v = (K_1, K_2, \dots)$ .

## Solution Techniques

Depending on the inversion grid discretization, the step in inversion (facies versus  $K$  estimation), and the number of conditioning measurements used, the system of equations can be underdetermined, exact, or overdetermined. For the problems of this study, all equation systems are overdetermined, because underdetermined problems generally yield poor or unstable solutions (Zhang 2014). Due to the nonlinearity in the LAS, the inversion system of equations is nonlinear and is solved using two gradient-based optimization algorithms, i.e., Levenberg-Marquardt and Trust-Region-Reflective. Both algorithms are implemented in the *MATLAB* nonlinear solver, *lsqnonlin*, which solves a nonlinear least-squares problem of the form

$$\min_{\mathbf{x}} \|f(\mathbf{x})\|_2^2 = \min_{\mathbf{x}} (f_1(\mathbf{x})^2 + f_2(\mathbf{x})^2 + \dots + f_w(\mathbf{x})^2) \quad (20)$$

where  $\mathbf{x}$  = inverse solution containing the unknown parameters and coefficients;  $w$  = number of equations; and  $f_1(\mathbf{x})$ ,  $f_2(\mathbf{x})$ ,  $\dots$ ,  $f_w(\mathbf{x})$  = equations assembled. The optimization algorithms require that an initial guess of  $\mathbf{x}$  be provided. In this work, the initial guess is generated by assigning to  $\mathbf{x}$  random values bounded by the range of the observed heads. Finally, the LAS-based inversion, similar to all inversion methods, can suffer ill-posedness when insufficient and/or noisy data are used to condition the inversion (Zhang 2014). This ill-posedness can be manifested as unstable or nonunique inversion solutions. With sufficient and accurate data that lead to exact or overdetermined equation systems, the inverse problems are generally well-posed, leading to fast, stable, and accurate solutions.

## Forward Transport Modeling

The transport equation describing the migration of a solute in aquifers can be written as

$$\frac{\partial c(x, y, t)}{\partial t} = \nabla \cdot [\mathbf{D} \cdot \nabla c(x, y, t)] - \nabla \cdot [\mathbf{v}c(x, y, t)] \quad \text{on } \Omega \quad (21)$$

$$c(x, y, 0) = 0 \quad \text{on } \Omega \quad (22)$$

$$c(x, y, t) = c_0(x, y) \quad \text{on } \Gamma_1, \quad t > 0 \quad (23)$$

where  $c$  = solute concentration;  $\mathbf{D}$  = dispersion tensor;  $\mathbf{v}$  = groundwater velocity, which is related to Darcy flux  $\mathbf{q} = [q_x(x, y), q_y(x, y)]$  via porosity  $\theta$  ( $\mathbf{v} = \mathbf{q}/\theta$ ); and  $\Gamma_1$  = Dirichlet solute BC approximating a constant-source contaminant release into the aquifer. Zero mass flux is imposed on the remaining boundaries.  $\mathbf{D}$  is related to local dispersivities via  $D_{ij} = [\alpha_T \delta_{ij} + (\alpha_L - \alpha_T)(v_i v_j / v^2)]v$ , where  $v_i$  is the  $i$ th component of  $\mathbf{v}$  whose magnitude is  $v$ ; and  $\alpha_L$  and  $\alpha_T$  are local longitudinal and transverse dispersivities, respectively. If porosity is assumed known, groundwater velocity can be obtained from the estimated  $\tilde{q}_x(x, y)$  and  $\tilde{q}_y(x, y)$  fields. In this study,  $\theta = 0.1$ . When dispersivities are also assumed known, contaminant migration can be predicted by solving Eqs. (21)–(23) in the forward mode given both the original and the inverted flow fields. In this study,  $\alpha_L = 0.1$  m and  $\alpha_T = \alpha_L/10$ .

## Results and Discussion

To test the inverse method, two synthetic aquifer models are simulated to solve Eq. (1) in the forward mode using *MODFLOW* (Harbaugh et al. 2000), which discretizes Eq. (1) with the finite-difference method. The forward-flow model is referred to herein as the finite-difference model (FDM). Facies patterns of these models are irregular (Problem 1) versus regular (Problem 2), with these conductivities:  $K_1 = 1$  m/day and  $K_2 = 10$  m/day (Problem 1), and 10, 20, 30, and 40 m/day (Problem 2). In both problems, domain size is  $L_x = 1,000$  m and  $L_y = 1,000$  m, discretized with  $100 \times 100$  grid cells in the FDM. Each model is driven by a set of true-flow BC:  $h(x, y = 0) = 10$  m;  $h(x, y = 1,000) = 20$  m; the remaining sides are no-flux. To obtain measurements for inversion, hydraulic heads, fluxes, or local  $K$  are sampled from the FDM in a regular gridded pattern. Fluxes and local  $K$  are sampled at the same locations. The inversion grid covers the same spatial extent as the FDM, although its discretization is much coarser. As shown in Zhang et al. (2014), extent of the inversion grid is determined by

the measurement locations only, which may span the dimensions of the forward model (this work), although this is not a requirement (the inversion grid does not need to extend to the natural aquifer boundaries). To evaluate the stability of inversion, increasing measurement errors are imposed on the data: the observed hydraulic heads ( $h^{\text{FDM}}$ ), Darcy fluxes ( $q^{\text{FDM}}$ ), and local conductivities ( $K^{\text{FDM}}$ ) are all corrupted by uniform noises:  $h^m = h^{\text{FDM}} \pm \Delta h$ ,  $q^m = q^{\text{FDM}} \pm \Delta q$ , and  $K^m = K^{\text{FDM}} \pm \Delta K$ , where  $h^m$ ,  $q^m$ , and  $K^m$  are measurements provided to inversion, and  $\Delta h$ ,  $\Delta q$ , and  $\Delta K$  are the corresponding measurement errors. The highest imposed error is  $\pm 5\%$  of the total head, flux, and conductivity variations in the forward model, respectively. In the following, the facies pattern and inverted hydraulic heads are obtained at the end of the first inversion step, while the velocity fields are obtained at the end of the second inversion step, i.e., after the  $K$  estimation is completed.

Inversion accuracy is determined by comparing the solution (i.e., the recovered  $K$  pattern, values, and the flow field) against those of the FDM. A root-mean square error (RMS) and a relative root-mean square error (RES) of hydraulic head are defined at the measurement locations as

$$\text{RMS}(h) = \sqrt{\frac{1}{N_t} \sum_{i=1}^{N_t} [h_{\text{true}}(x_i, y_i) - h(x_i, y_i)]^2} \quad (24)$$

$$\text{RES}(h) = \frac{\sqrt{\sum_{i=1}^{N_t} [h_{\text{true}}(x_i, y_i) - h(x_i, y_i)]^2}}{\sqrt{\sum_{i=1}^{N_t} [h_{\text{true}}(x_i, y_i)]^2}} \quad (25)$$

where  $h_{\text{true}}(x_i, y_i)$  = measured heads from the FDM;  $h(x_i, y_i)$  = inverted hydraulic head at the same measurement location; and  $N_t$  = total number of measured hydraulic heads. For facies comparison, a similarity index is expressed as

$$\text{Similarity Index} = \frac{\text{total}E}{\text{total}G} \quad (26)$$

where  $\text{total}E$  = number of grid cells where the facies type is correctly recovered by inversion; and  $\text{total}G$  = total number of cells.

For each inversion problem, given the original and the recovered flow fields, contaminant migration is simulated over time to predict solute concentration in the aquifer using a modular three-dimensional multispecies transport model (MT3DMS) (Zheng 2010). The transport model is of the same dimensions as the flow model ( $L_x = 1,000$  m and  $L_y = 1,000$  m), and is discretized with  $100 \times 100$  grid cells. In these experiments, the same porosity, dispersivities, and solute initial and BC are used. The transport model is simulated for a sufficiently long time and is terminated at 10,000 days when solute concentration in the forward (true) flow field has reached steady-state. The same termination time is used

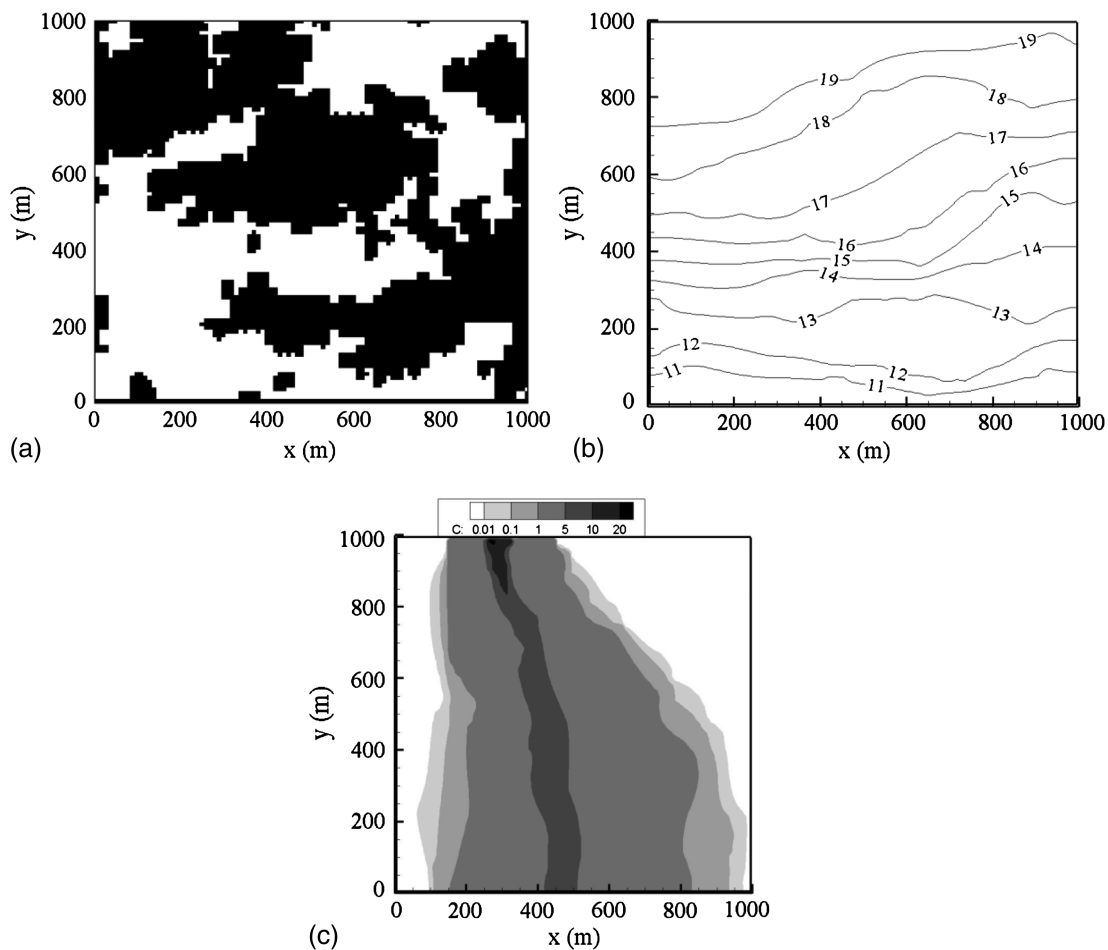


**Fig. 2.** Forward model of Problem 1 with two facies (black facies:  $K = 10$  m/day; white facies:  $K = 1$  m/day): (a) true conductivity pattern (Reprinted from Journal of Computational Physics, Vol. 229, H. Chang, D. Zhang, and Z. M. Lu, “History matching of facies distribution with the EnKF and level set parameterization,” pp. 91–102, Copyright 2010, with permission from Elsevier); (b) distribution of the true hydraulic head (unit: m); (c) distribution of true solute concentration (unit: mg/L at  $t = 10,000$  day)

**Table 1.** Inversion Cases for Problem 1 (Two Facies)

Inverse case	Number of observed data points			Inversion grid	Errors in the observed data (%)	Estimated conductivities			Similarity index	
	Head	Flux	Local $K$			$K1$ (true) = 1.00	$K2$ (true) = 10.00	RMS (h)		RES (h)
Case 1	100	100	0	$5 \times 5$	0	1.74	9.12	0.23	0.014	0.75
					$\pm 1$	1.70	9.04	0.23	0.015	0.74
					$\pm 5$	1.76	9.12	0.30	0.019	0.72
Case 2	100	0	100	$5 \times 5$	0	1.00	10.00	0.23	0.015	0.82
					$\pm 1$	1.00	10.00	0.24	0.015	0.82
					$\pm 5$	1.00	10.01	0.29	0.018	0.82
Case 3	36	36	0	$3 \times 3$	0	2.27	8.96	0.34	0.022	0.64
					$\pm 1$	2.41	7.51	0.35	0.022	0.64
					$\pm 5$	2.26	7.25	0.46	0.029	0.61
Case 4	36	0	36	$3 \times 3$	0	1.00	10.00	0.33	0.021	0.74
					$\pm 1$	1.00	9.99	0.34	0.022	0.74
					$\pm 5$	1.00	9.98	0.45	0.028	0.74

Note: When errors are imposed, all the measured heads, fluxes, or local  $K$ s are subject to the errors; estimated facies  $K$ s (m/day) and observed  $K$  (m/day) are listed; head is given in m; observed flux is given in m/day.

for transport modeling in the inverted flow fields. Moreover, along the outflow boundary, concentration breakthrough over time is computed by averaging the concentrations predicted at all grid cells.

### Problem 1 (Two Facies)

The forward model consists of two irregularly shaped facies [Fig. 2(a)]. For the chosen fluid flow BC, true hydraulic head distribution is computed [Fig. 2(b)]. Transport is then modeled, for which the concentration distribution at steady-state is shown [Fig. 2(c)].

By varying measurement size, type, errors, and grid discretization, four inversion cases are tested (Table 1). Cases 1 and 2 share the same inversion grid and the number of measurements. For Case 1, fluxes are sampled and provided to inversion; for Case 2, local  $K$ s are used instead. For both cases, observed heads are sampled at the same locations. To first identify facies,  $K_0$  is varied from 4.0 to 6.0, which yields nearly identical facies patterns; thus, only one set of results (at  $K_0 = 5$ ) is presented. After the facies is identified, inversion is repeated using the same measurements and Eqs. (17)–(19) to estimate the conductivities. The problem setups

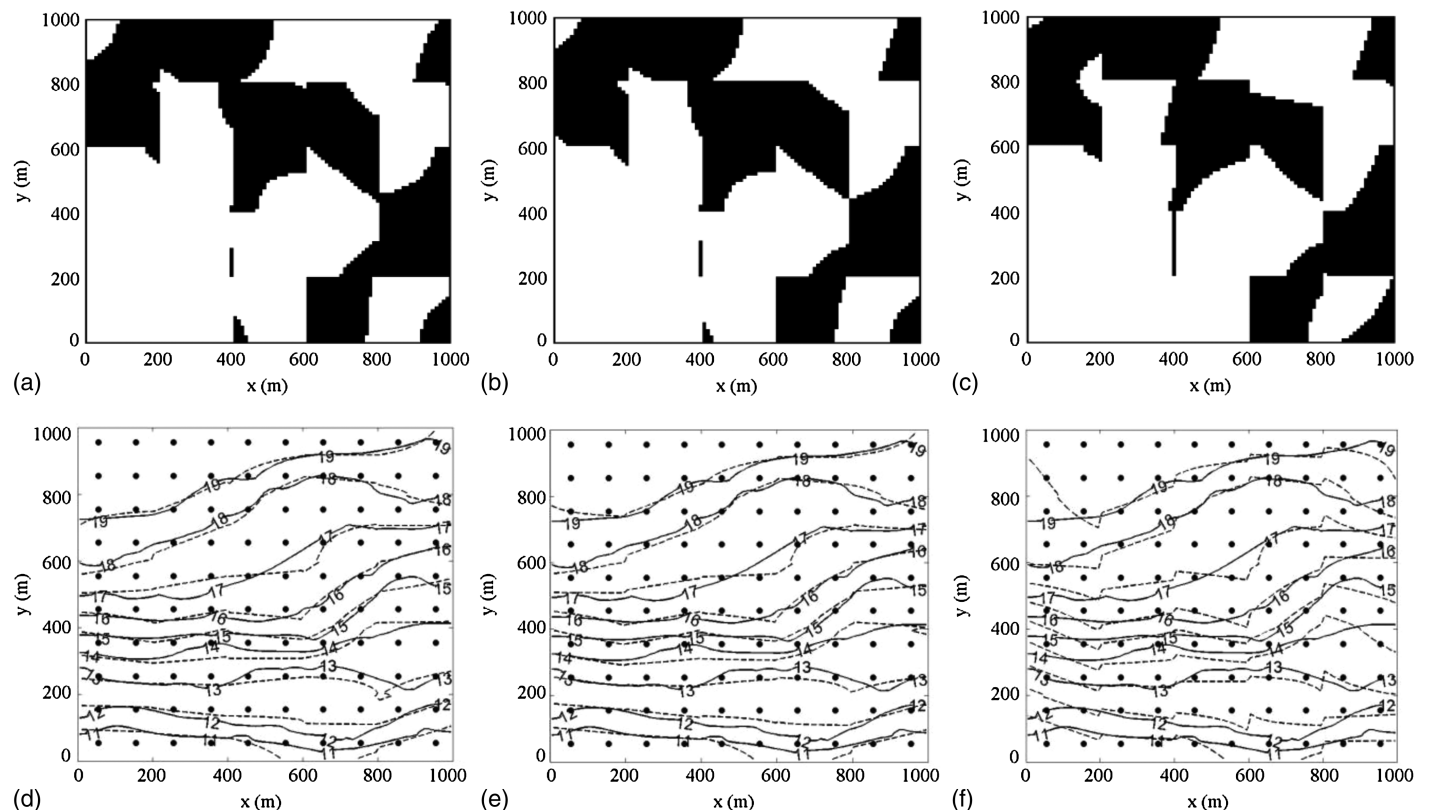


**Fig. 3.** Case 1 under increasing measurement errors: (a) through (c) show inverted facies patterns and (d) through (f) show hydraulic head fields (head unit: m; dashed line indicates true hydraulic heads; dashed-dotted line indicates inverted hydraulic heads; solid circles indicate locations of observed heads and fluxes): (a) 0% error; (b)  $\pm 1\%$  error; (c)  $\pm 5\%$  error; (d) 0% error; (e)  $\pm 1\%$  error; (f)  $\pm 5\%$  error

for Cases 3 and 4 are similar, although fewer measurements are used while inversion grid is also coarsened. The same  $K_0$  value is used. For all cases, the estimated facies  $K$  values and hydraulic head field degrade with increasing measurement errors, as expected, although the inverted facies pattern is relatively insensitive to errors (Figs. 3–6). For the range of the error magnitude tested, inversion outcome is overall very stable, i.e., estimation error remains bounded under increasing measurement errors. Given the inverted velocity fields (not plotted), results of transport modeling are then compared. The four cases will now be presented and discussed in greater detail.

For Cases 1 and 2, the recovered facies patterns and hydraulic head fields are shown in Figs. 3 and 4. The estimated facies conductivities are listed in Table 1, along with the  $RMS(h)$ ,  $RES(h)$ , and the similarity index. The similarity index varies from 0.72 at the highest error in the observed heads to 0.75 when observed heads are error-free for Case 1. Thus, facies recovery degrades slightly with increasing measurement errors, as expected. The overall facies patterns are captured in both cases when compared to Fig. 2(a), but not the fine detail. Comparing the two cases, Case 2 appears to be slightly better at recovering the facies pattern (its average similarity index is higher), while its estimated  $K$ s are also more accurate given the same measurement error (Table 1). The estimated  $K_1$  in Case 1 has the highest accuracy at  $\pm 1\%$  noise compared to the same  $K_1$  estimated under error-free conditions. Such an anomaly can be attributed to the fact that many factors influence inversion accuracy, e.g., weighting function, approximation function, number of collocation points, and quality, quantity, and position of the measurements, and the relative error imposed is small. Moreover,  $RMS(h)$  and  $RES(h)$  of the recovered heads at

the measurement locations appear similar for the two cases. These metrics appear less sensitive to the type of the measurements ( $K$ s versus fluxes) used to condition the inversion.

For Cases 3 and 4, fewer measurements and a coarser grid are used. The recovered facies patterns, head fields, and hydraulic conductivities are less accurate compared to those of Cases 1 and 2, although the coarsest facies' features are captured reasonably well (Figs. 5 and 6). The average similarity index ranges from 0.63 (Case 3) to 0.74 (Case 4) (Table 1). Comparing the two cases, Case 4 more accurately estimates the conductivity values, while it also better capture facies pattern. Again, when local  $K$ s are used to condition inversion, both facies and  $K$  estimations are more accurate. Moreover, the estimated Dirichlet BC, sampled along the inversion grid boundary from (0, 0), (1000, 0), (1000, 1000), (0, 1000), to (0, 0), are compared between the cases (Fig. 7). Although BC recovery generally degrades with decreasing measurements and increasing errors, overall, BC recovery is similar and is relatively insensitive to the errors of the observed data.

Given the recovered flow fields, solute concentration in the aquifer at  $t = 10,000$  days is shown (Fig. 8), which can be compared to that simulated with the true flow field [Fig. 2(c)]. In both transport simulations, a constant solute mass flux is specified near the inflow boundary at  $x = 150\text{--}450$  m,  $y = 995$  m. At the outflow boundary, comparison of concentration breakthrough is also presented (Fig. 9). Both concentration distribution and breakthrough predicted with the recovered velocity field of Case 1 are more accurate than those of Case 2. When measurements are reduced, as in Cases 3 and 4, plume prediction suffers greater inaccuracy, as does the computed breakthrough curve. Between the two, the predicted extent of the plume does not differ significantly, although the

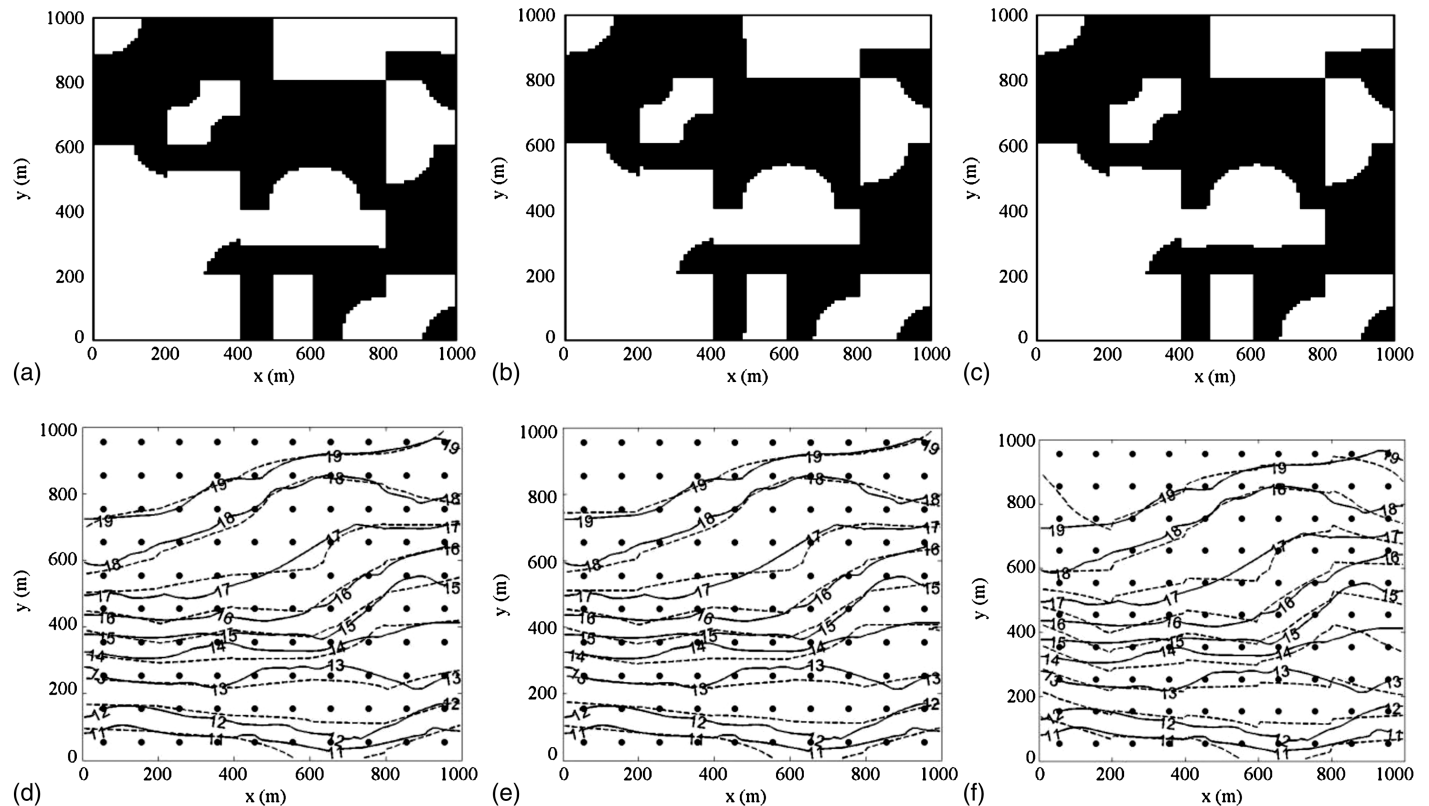


**Fig. 4.** Case 2 under increasing measurement errors: (a) through (c) show inverted facies patterns and (d) through (f) show hydraulic head fields (head unit: m; dashed line indicates true hydraulic heads; dashed-dotted line indicates inverted hydraulic heads; solid circles indicate locations of observed heads and local conductivities): (a) 0% error; (b)  $\pm 1\%$  error; (c)  $\pm 5\%$  error; (d) 0% error; (e)  $\pm 1\%$  error; (f)  $\pm 5\%$  error

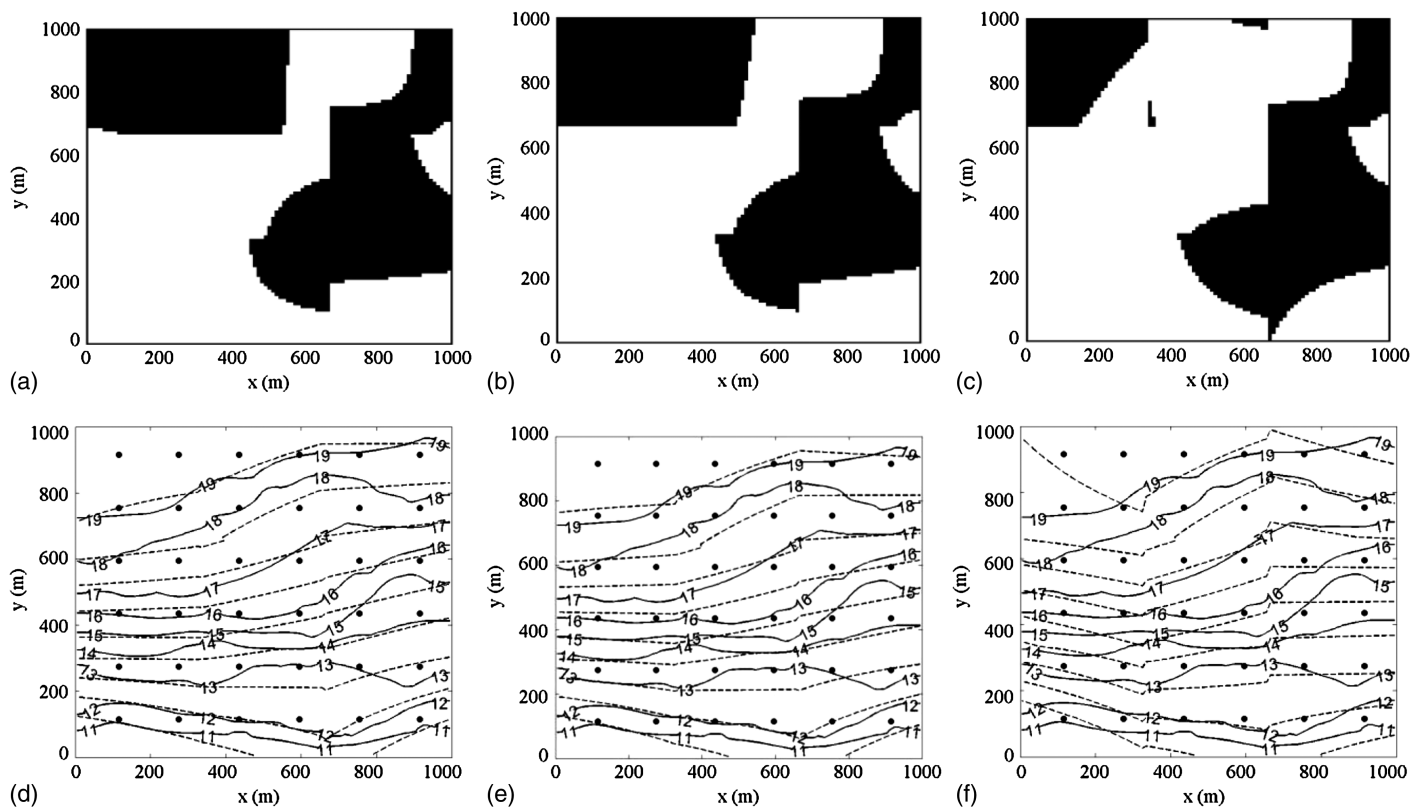


**Fig. 5.** Case 3 under increasing measurement errors: (a) through (c) show inverted facies patterns and (d) through (f) show hydraulic head fields (head unit: m; dashed line indicates true hydraulic heads; dashed-dotted line indicates inverted hydraulic heads; solid circles indicate locations of observed heads and fluxes): (a) 0% error; (b)  $\pm 1\%$  error; (c)  $\pm 5\%$  error; (d) 0% error; (e)  $\pm 1\%$  error; (f)  $\pm 5\%$  error

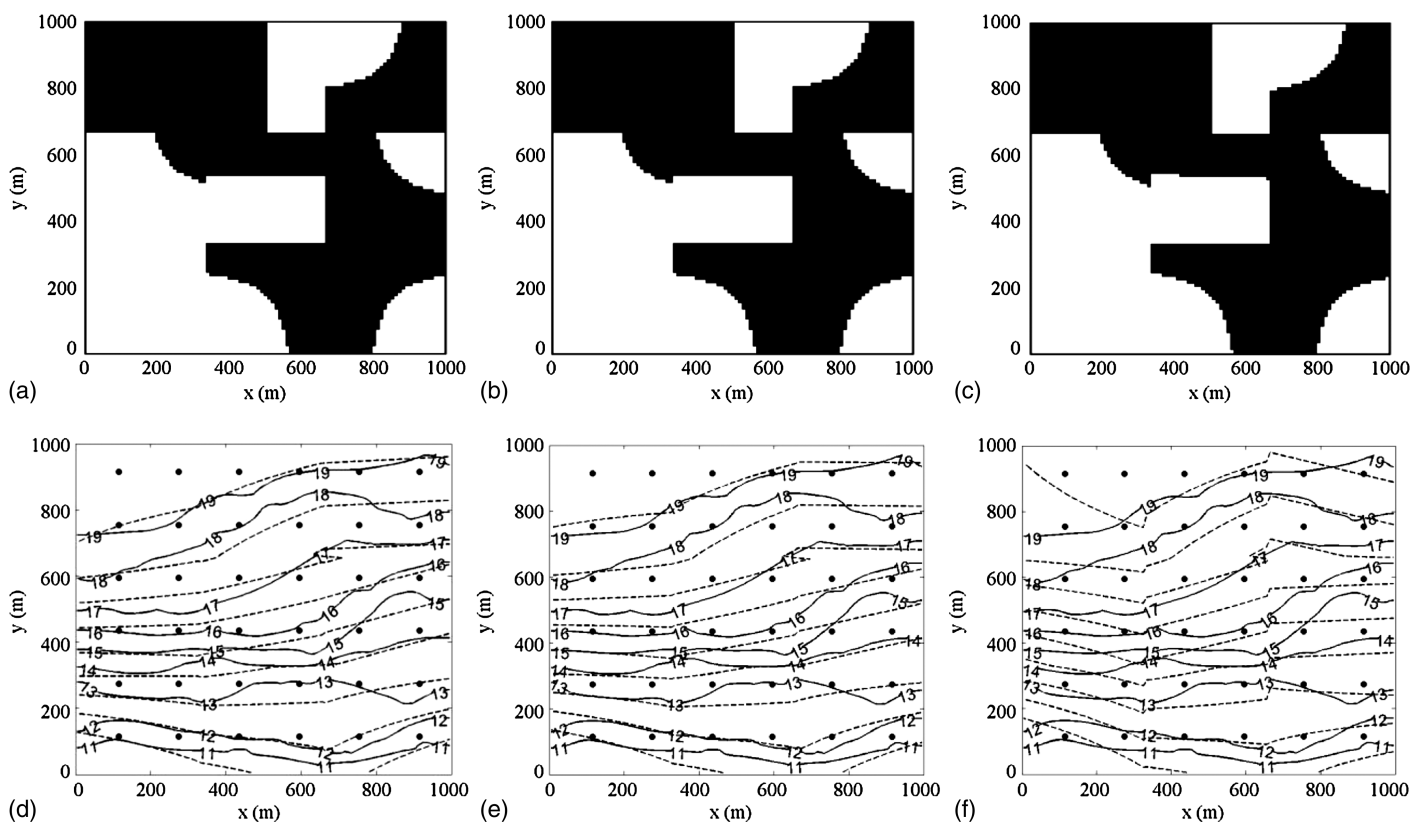


**Fig. 6.** Case 4 under increasing measurement errors: (a) through (c) show inverted facies patterns and (d) through (f) show hydraulic head fields (head unit: m; dashed line indicates true hydraulic heads; dashed-dotted line indicates inverted hydraulic heads; solid circles indicate locations of observed heads and local conductivities): (a) 0% error; (b)  $\pm 1\%$  error; (c)  $\pm 5\%$  error; (d) 0% error; (e)  $\pm 1\%$  error; (f)  $\pm 5\%$  error

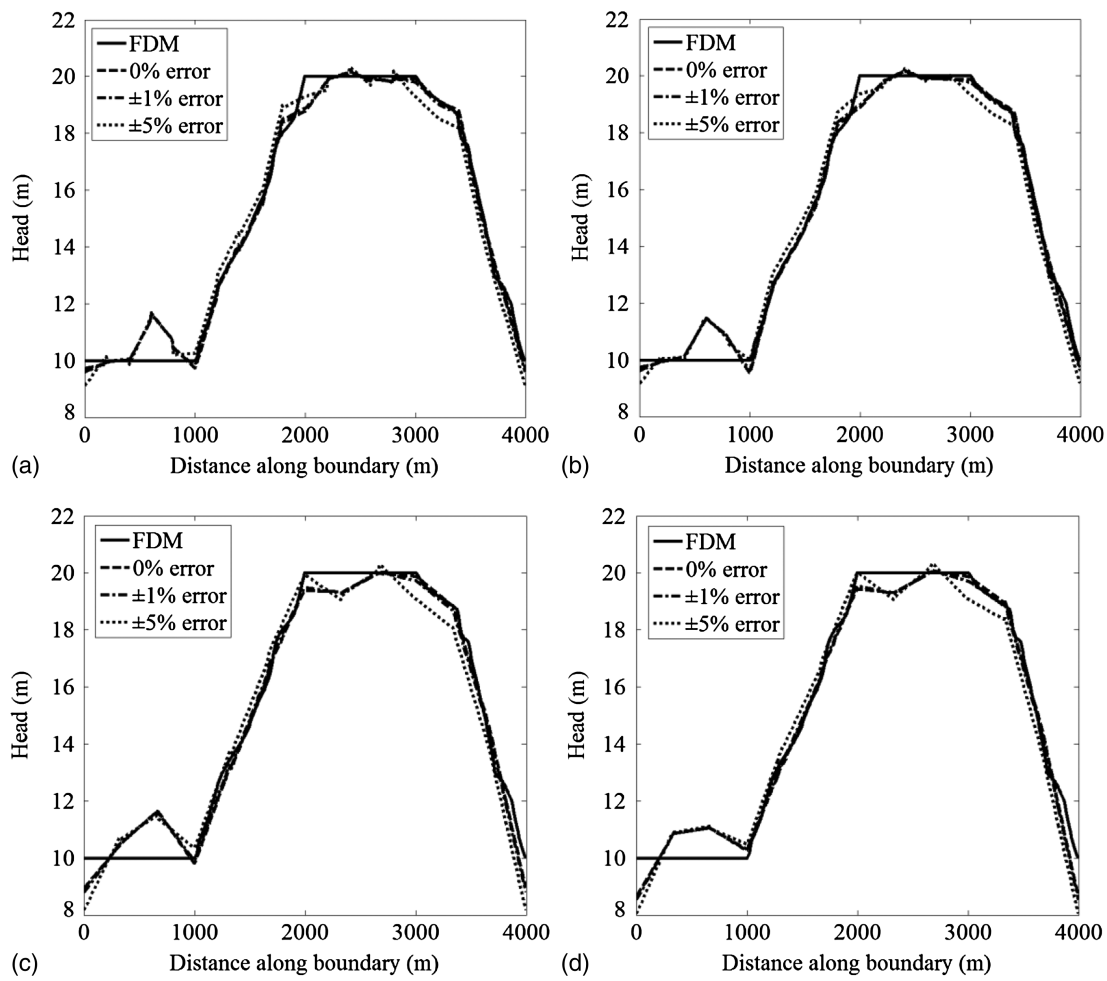


**Fig. 7.** Inverted hydraulic heads along model boundaries [sampled along the inversion grid boundary from (0, 0), (1000, 0), (1000, 1000), (0, 1000), to (0, 0)] for Cases 1–4 under increasing measurement errors: (a) Case 1; (b) Case 2; (c) Case 3; (d) Case 4

velocity field of Case 3 leads to more accurate breakthrough prediction. Interestingly, for any of the cases, with minor exceptions, transport prediction is not very sensitive to the imposed random measurement errors. Because Cases 1 and 3 are conditioned by local flux measurements while Cases 2 and 4 are conditioned by local  $K$  measurements, comparison of these problem cases indicates that flux conditioning can lead to more accurate velocity recovery. Unlike the local conductivity measurement, which itself does not contain information on the local hydraulic gradient, flux contains information on both the hydraulic gradient and local conductivity, which is shown here to be important for accurate velocity recovery.

### Problem 2 (Four Facies)

The FDM, of the same dimensions and discretization of Problem 1, contains four facies bounded by linear interfaces [Fig. 10(a)]. Given the same fluid flow BC of Problem 1, the true hydraulic head distribution can be computed [Fig. 10(b)]. Two inversion cases, sharing the same total number of measurements and grid, are evaluated (Table 2). For facies recognition, a set of threshold conductivities is selected as [15, 25, 35], which is considered a set of prior information constraints. While inversion for Case 5 is conditioned to fluxes, that of Case 6 is conditioned to local  $K$ s. The recovered facies patterns appear reasonable (Figs. 11 and 12), again, facies recognition is not sensitive to increasing measurement error, as the similarity index does not vary significantly with error (Table 2).

Similar to Problem 1, Case 6, by conditioning to local  $K$ s, yields more accurate delineation of facies boundaries, facies  $K$ s, and the hydraulic head field. Its average similarity index is 0.89, which is higher than that of Case 5. Inversion outcomes are also stable when measurement error is increased.

Given the original and the inverted flow fields, transport modeling is carried out next. The same porosity, dispersivities, and model domain size/discretization of Problem 1 are used. The location of contaminant release, identically assigned to all models, is slightly modified at  $x = 300\text{--}700$  m and  $y = 995$  m. Transport simulation is run for 2,000 days, at which time steady conditions are reached in all models. Fig. 13 shows computed solute breakthrough curves at the outflow boundary; those predicted using the inverted velocity fields are very accurate whether inversion is conditioned on fluxes or local  $K$ s. The same accuracy is also accomplished in the capture of the plume shape by both cases. Compared to the tortuous flow paths of Problem 1, which arise from irregular facies distribution, those of Problem 2 are relatively smooth-varying. This yields the inverted velocity fields that are all relatively close to that of the true model, yielding accurate transport predictions. Because Problem 1 (Cases 1 and 2) and Problem 2 employ a similar measurement support and an identical inversion grid, accuracy of the inverted velocity and thus transport prediction is sensitive to  $K$  heterogeneity: a more-irregular facies pattern is more challenging to invert.

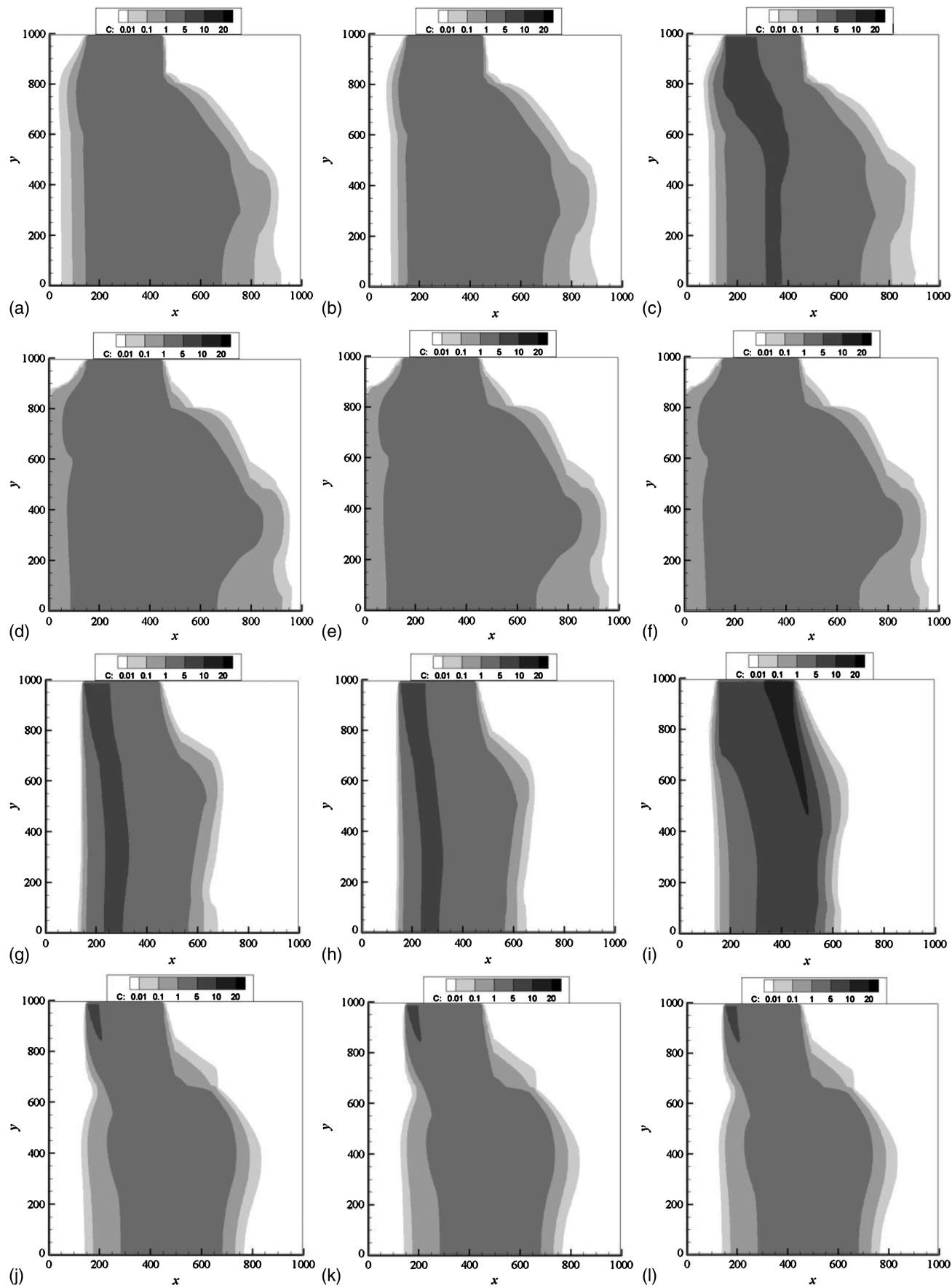


**Fig. 8.** Modeled concentration (in mg/L) at  $t = 10,000$  day given the recovered flow fields of Problem 1 (two facies): (a) 0% error (Case 1); (b)  $\pm 1\%$  error (Case 1); (c)  $\pm 5\%$  error (Case 1); (d) 0% error (Case 2); (e)  $\pm 1\%$  error (Case 2); (f)  $\pm 5\%$  error (Case 2); (g) 0% error (Case 3); (h)  $\pm 1\%$  error (Case 3); (i)  $\pm 5\%$  error (Case 3); (j) 0% error (Case 4); (k)  $\pm 1\%$  error (Case 4); (l)  $\pm 5\%$  error (Case 4)

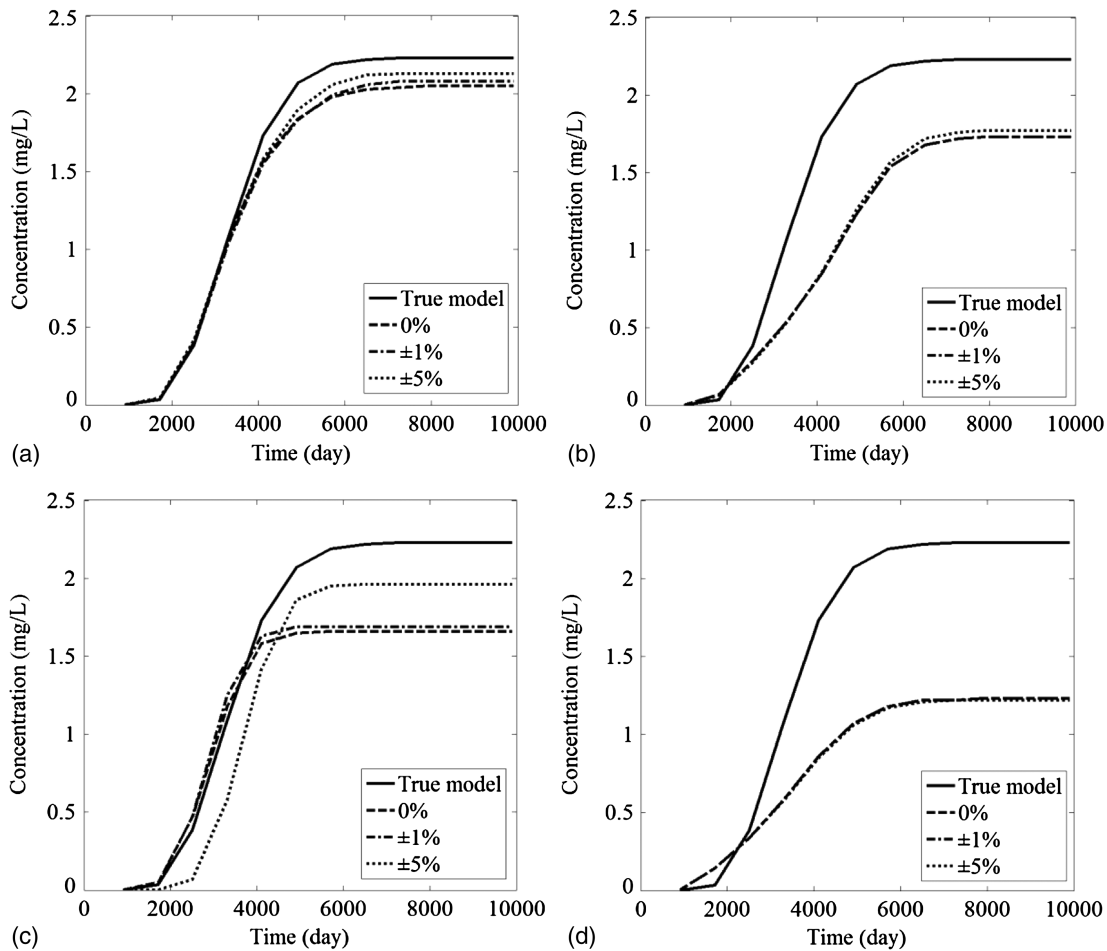


**Fig. 9.** Concentration breakthrough at the outflow boundary for Problem 1: (a) Case 1; (b) Case 2; (c) Case 3; (d) Case 4

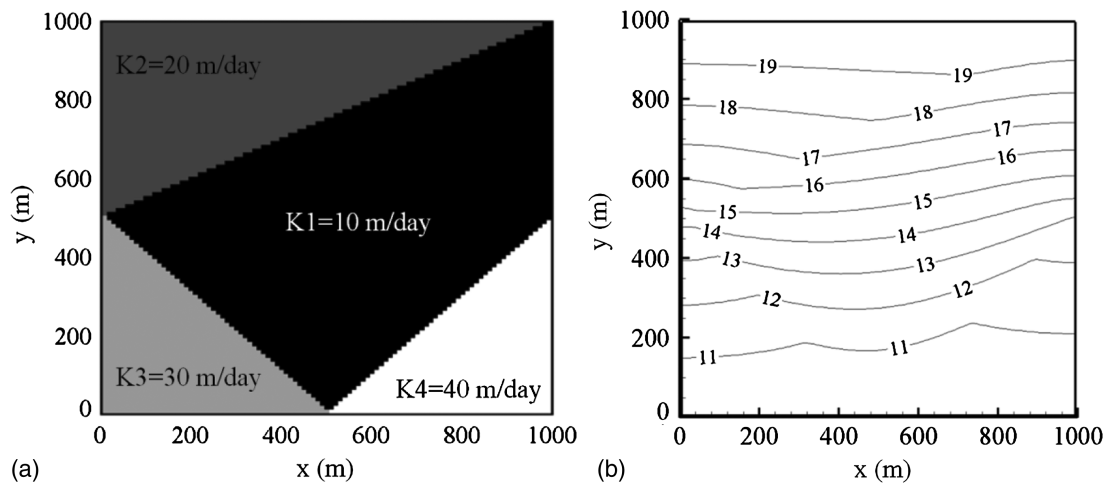


**Fig. 10.** Forward model of Problem 2 with four facies: (a) true conductivity pattern; (b) true distribution of the hydraulic head (unit: m)

## Conclusions

Parameter structure identification with a direct inverse method is proposed for estimating subsurface hydraulic conductivity pattern, values, and the associated flow field under unknown aquifer fluid-flow boundary conditions. To facilitate inversion, different local approximate solutions (LAS) of the governing flow equation are proposed. Given the LAS, inversion imposes fluid-flow continuity

conditioned to limited measurements (e.g., heads, fluxes, or local conductivities), while enforcing flow physics at discrete spatial locations, thus making the inverse problem well-posed. Hydraulic conductivity is formulated as piecewise continuous functions which, along with a set of threshold values as prior information constraints, can be used to facilitate facies recognition. Because forward-flow simulations are not required in order to minimize measurement-to-model misfits, knowledge of aquifer BC is not

**Table 2.** Inversion Cases for Problem 2 (Four Facies)

Inverse case	Number of observed data points			Inversion grid	Errors in the observed data (%)	Estimated conductivity				RMS (h)	RES (h)	Similarity pattern
	Head	Flux	Local $K$			$K1$ (true) = 10.00	$K2$ (true) = 20.00	$K3$ (true) = 30.00	$K4$ (true) = 40.00			
Case 5	100	100	0	$5 \times 5$	0	10.39	20.6	31.25	41.53	0.056	0.0037	0.83
					$\pm 1$	10.39	20.54	30.82	41.55	0.067	0.0045	0.83
					$\pm 5$	10.44	21.39	32.16	42.76	0.19	0.013	0.80
Case 6	100	0	100	$5 \times 5$	0	10.00	20.00	30.00	40.00	0.057	0.0038	0.89
					$\pm 1$	10.01	19.96	29.94	40.08	0.067	0.0045	0.89
					$\pm 5$	10.04	19.80	29.70	40.40	0.19	0.013	0.89

Note: When errors are imposed, all the measured heads, fluxes, or local  $K$ s are subject to the errors; estimated facies  $K$ s (m/day) and observed  $K$  (m/day) are listed; head is given in m; observed flux is given in m/day.

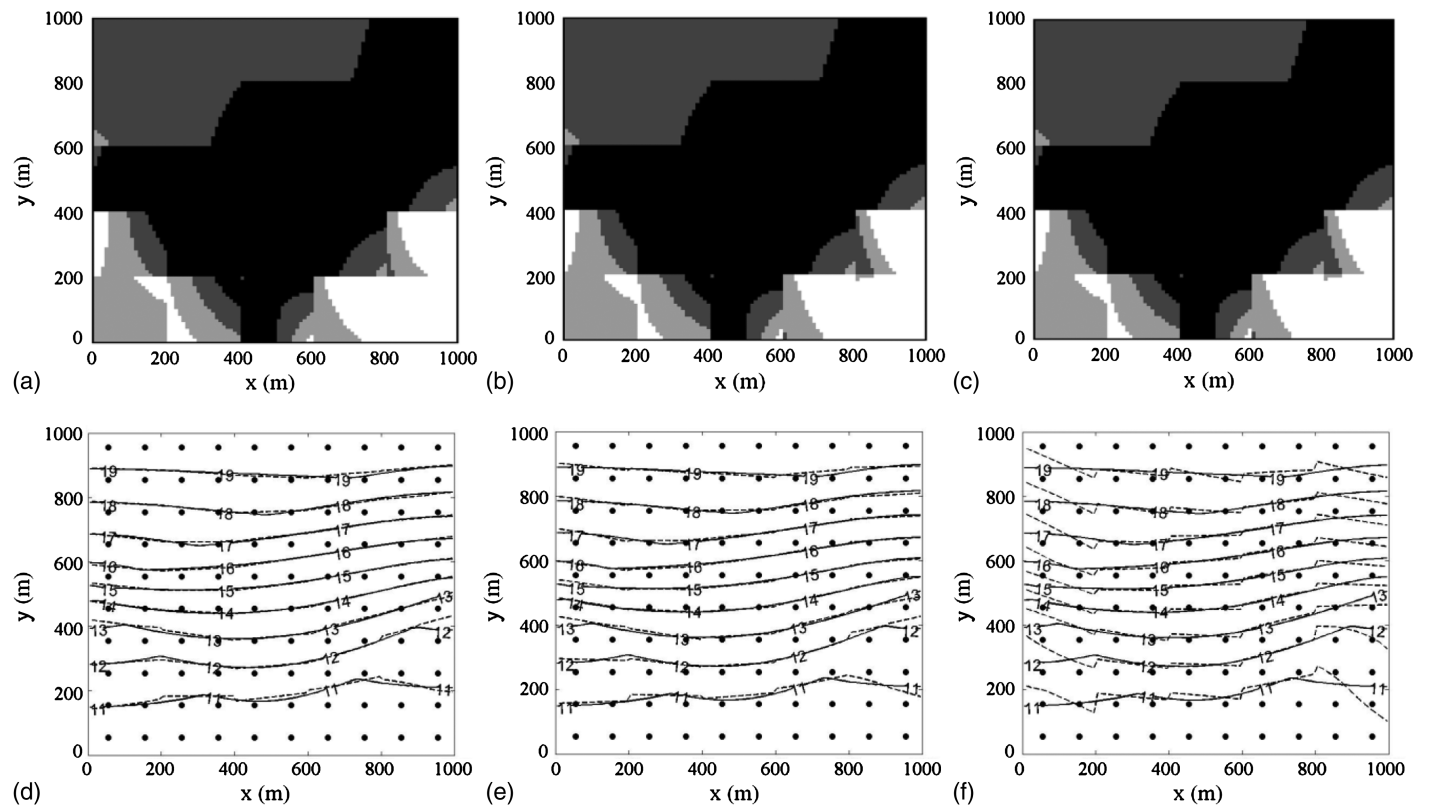


**Fig. 11.** Case 5 under increasing measurement errors: (a) through (c) show inverted facies patterns, where grayscale colors represent facies associated with the distinct  $K$  values in Fig. 10(a), and (d) through (f) show hydraulic head fields (unit: m; dashed line indicates true hydraulic heads; dashed-dotted line indicates inverted hydraulic heads; solid circles indicate locations of observed heads and fluxes): (a) 0% error; (b)  $\pm 1\%$  error; (c)  $\pm 5\%$  error; (d) 0% error; (e)  $\pm 1\%$  error; (f)  $\pm 5\%$  error

needed. The inverse method therefore differs significantly from the majority of inversion techniques, which require the repeated simulations of the forward model under assumed (known) BC. Instead, a single set of inversion equations is assembled and solved with optimization, and thus the method is computationally efficient. Moreover, given the inverted flow field, estimated based on hydraulic measurements alone, transport modeling of contaminant release can be carried out. Results of this study are summarized as follows:

1. By formulating hydraulic conductivity as piecewise continuous functions (one for each inversion grid cell), the inverse method can recognize large-scale facies patterns;

2. The estimated facies, their  $K$  values, and the associated flow field become less accurate with increasing measurement errors, decreasing measurement support, and coarsened inversion grid. Fine-scale facies pattern can be recovered only with extremely high measurement support;
3. For all the cases considered, the inverse solution is stable with increasing measurement errors, i.e., estimation errors remain bounded while the facies pattern obtained is relatively insensitive to errors. When error is at its highest, inversion is able to capture the largest scale facies feature and thus the overall flow field;
4. Contaminant transport pathway and breakthrough can be captured given the inverted flow field, although transport prediction

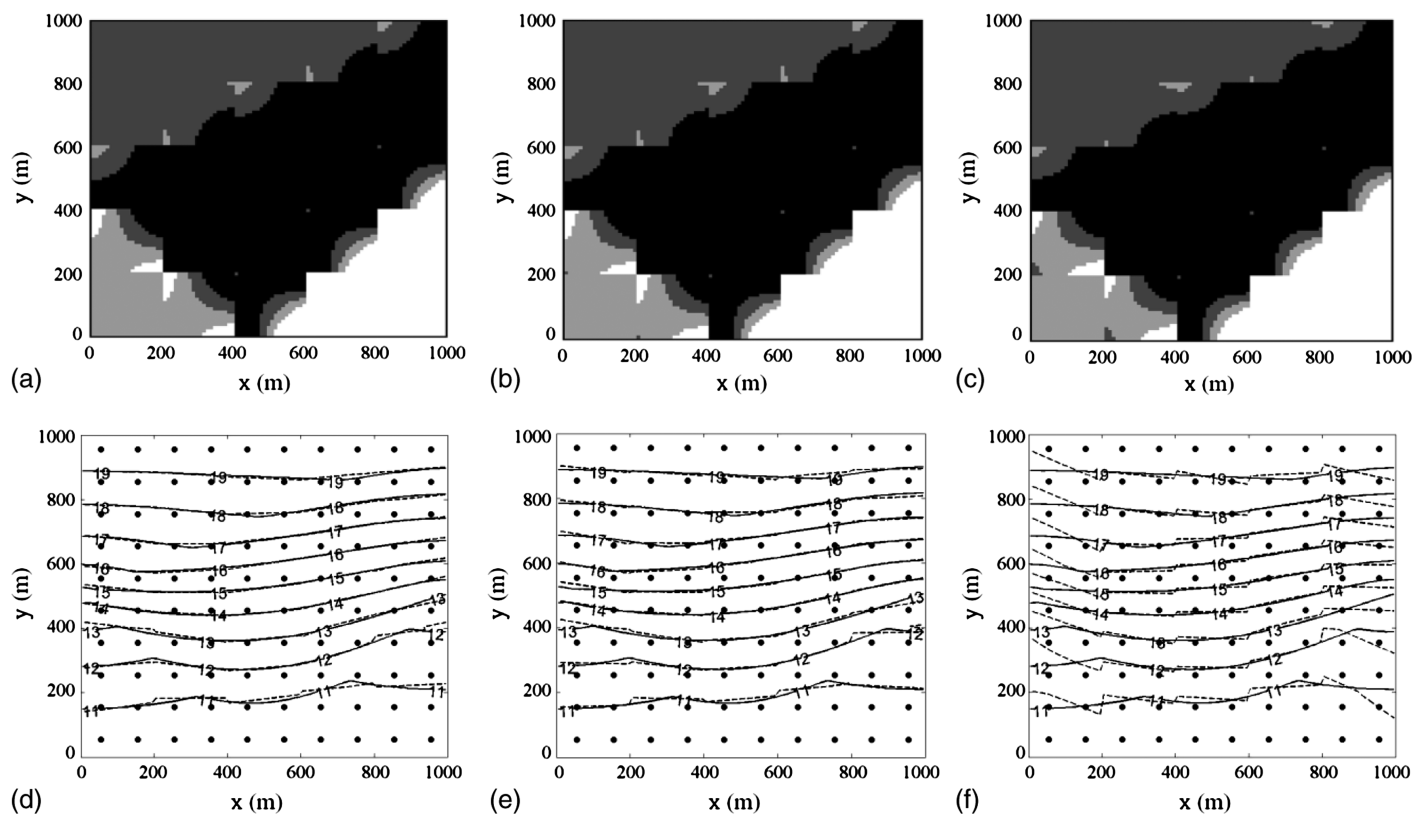


**Fig. 12.** Case 6 under increasing measurement errors: (a) through (c) show inverted facies patterns, where grayscale colors represent facies associated with the distinct  $K$  values in Fig. 10(a), and (d) through (f) show hydraulic head fields (unit: m; dashed line indicates true hydraulic heads; dashed-dotted line indicates inverted hydraulic heads; solid circles indicate locations of observed heads and local conductivities): (a) 0% error; (b)  $\pm 1\%$  error; (c)  $\pm 5\%$  error; (d) 0% error; (e)  $\pm 1\%$  error; (f)  $\pm 5\%$  error

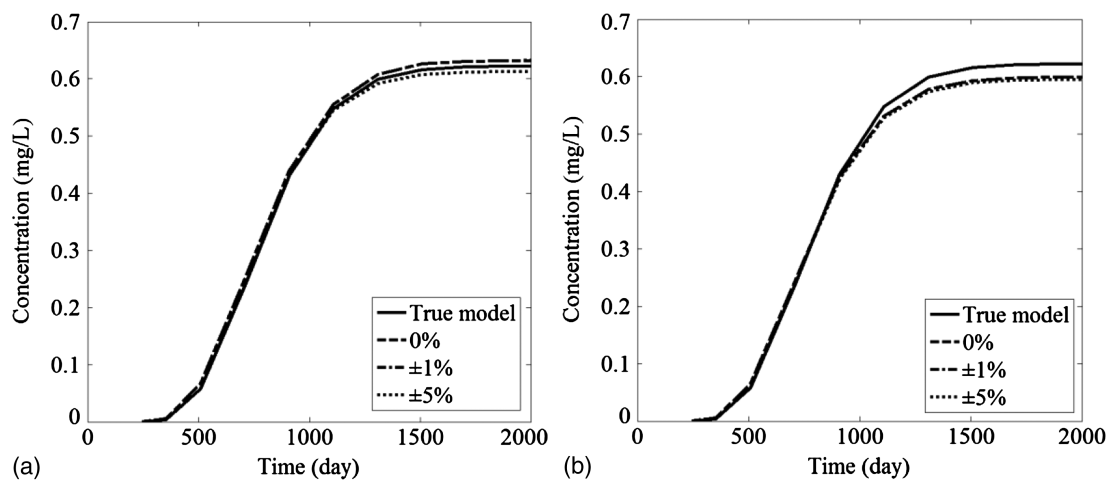


**Fig. 13.** Concentration breakthrough at the outflow boundary for Problem 2 (four facies): (a) Case 5; (b) Case 6

is less accurate when facies pattern is more strongly irregular; and

- Local conductivity and Darcy flux measurements have similar information content, although inversion outcomes exhibit subtle differences: local  $K$ s lead to better identification of facies pattern, conductivity values, and hydrological state; Darcy fluxes lead to better identification of the velocity field, and thus to more-accurate predictions of solute concentration and breakthrough curve.

For aquifers with unknown fluid flow boundary conditions, the inverse method of this study utilizes hydraulic measurements alone to determine subsurface conductivity distribution and to predict contaminant migration in aquifers. Only the overall facies pattern can be recovered, however, without incurring great sampling costs. To improve on this work and to better resolve fine-scale facies features, future work will pursue transient flow inversion under pumping and/or injection or joint flow and transport inversion. In these cases, new constraints will be provided by adding time-dependent

hydraulic and/or solute concentration measurements. By incorporating stochastic techniques, future work will quantify uncertainty in estimating both parameters and flow field. As shown in Jiao and Zhang (2015a), a trade-off between measurement support and uncertainty exists, thus data requirements can be reduced at the cost of creating uncertainty in inversion.

## Acknowledgments

This work is supported by the University of Wyoming's Center for Fundamentals of Subsurface Flow of the School of Energy Resources (WYDEQ49811ZHNG) and NSF EPSCoR (EPS 1208909).

## References

- Alcolea, A., Carrera, J., and Medina, A. (2006a). "Inversion of heterogeneous parabolic-type equations using the pilot points method." *Int. J. Numer. Methods Fluids*, 51(9–10), 963–980.
- Alcolea, A., Carrera, J., and Medina, A. (2006b). "Pilot points method incorporating prior information for solving the groundwater flow inverse problem." *Adv. Water Resour.*, 29(11), 1678–1689.
- Bennet, A. F. (1992). *Inverse methods in physical oceanography*, Cambridge University Press, New York.
- Carrera, J., Alcolea, A., Medina, A., Hidalgo, J., and Slooten, L. J. (2005). "Inverse problem in hydrogeology." *Hydrogeol. J.*, 13(1), 206–222.
- Carrera, J., and Neuman, S. P. (1986a). "Estimation of aquifer parameters under transient and steady state conditions: 3. Application to synthetic and field data." *Water Resour. Res.*, 22(2), 228–242.
- Carrera, J., and Neuman, S. P. (1986b). "Estimation of aquifer parameters under transient and steady-state conditions. 1. Maximum likelihood method incorporating prior information." *Water Resour. Res.*, 22(2), 199–210.
- Certes, C., and de Marsily, G. (1991). "Application of the pilot point method to the identification of aquifer transmissivities." *Adv. Water Resour.*, 14(5), 284–300.
- Chang, H., Zhang, D., and Lu, Z. M. (2010). "History matching of facies distribution with the EnKF and level set parameterization." *J. Comput. Phys.*, 229(20), 8011–8030.
- Dai, Z., and Samper, J. (2004). "Inverse problem of multicomponent reactive chemical transport in porous media: Formulation and applications." *Water Resour. Res.*, 40(7), W07407.
- de Marsily, G. (1978). "De l'identification des systemes en hydrogeologies." Ph.D. thesis, Pierre and Marie Curie Univ., Paris (in French).
- Ginn, T. R., and Cushman, J. H. (1990). "Inverse methods for subsurface flow: A critical review of stochastic techniques." *Stochastic Hydrol. Hydraul.*, 4(1), 1–26.
- Gomez-Hernandez, J. J., Sahuquillo, A., and Capilla, J. E. (1997). "Stochastic simulation of transmissivity fields conditional to both transmissivity and piezometric data—I: Theory." *J. Hydrol.*, 203(1–4), 162–174.
- Harbaugh, A. W., Banta, E. R., Hill, M. C., and McDonald, M. G. (2000). "MODFLOW-2000, the U.S. Geological Survey modular ground-water model—User guide to modularization concepts and the ground-water flow process." *Rep. 00-92, 121*, U.S. Geological Survey, Reston, VA.
- Hernandez, A. F., Neuman, S. P., Guadagnini, A., and Carrera, J. (2006). "Inverse stochastic moment analysis of steady state flow in randomly heterogeneous media." *Water Resour. Res.*, 42(5), W05425.
- Hill, M. C., and Tiedeman, C. R. (2007). *Effective groundwater model calibration: With analysis of data, sensitivities, predictions, and uncertainty*, Wiley, New York.
- Irsa, J., and Zhang, Y. (2012). "A new direct method of parameter estimation for steady state flow in heterogeneous aquifers with unknown boundary conditions." *Water Resour. Res.*, 48(9), W09526.
- Jiao, J. Y., and Zhang, Y. (2014a). "A method based on local approximate solutions (LAS) for inverting transient flow in heterogeneous aquifer." *J. Hydrol.*, 514, 145–149.
- Jiao, J. Y., and Zhang, Y. (2014b). "Two-dimensional inversion of confined and unconfined aquifers under unknown boundary condition." *Adv. Water Resour.*, 65, 43–57.
- Jiao, J. Y., and Zhang, Y. (2015a). "Functional parameterization for hydraulic conductivity inversion with uncertainty quantification." *Hydrogeol. J.*, 23(3), 597–610.
- Jiao, J. Y., Zhang, Y. (2015b). "Tensor hydraulic conductivity estimation for heterogeneous aquifers under unknown boundary conditions." *Groundwater*, 53(2), 293–304.
- Kurapov, A. L., Egbert, G. D., Allen, J. S., and Miller, R. N. (2007). "Representer-based variational data assimilation in a nonlinear model of nearshore circulation." *J. Geophys. Res.: Oceans*, 112(C11), C11019.
- Lu, Z., and Robinson, B. A. (2006). "Parameter identification using the level set method." *Geophys. Res. Lett.*, 33(6), L06404.
- MATLAB version 8.0 [Computer software]. MathWorks, Natick, MA.
- McLaughlin, D., and Townley, L. R. (1996). "A reassessment of the groundwater inverse problem." *Water Resour. Res.*, 32(5), 1131–1161.
- Ngodock, H. E., Jacobs, G. A., and Chen, M. S. (2006). "The representer method, the ensemble Kalman filter and the ensemble Kalman smoother: A comparison study using a nonlinear reduced gravity ocean model." *Ocean Modell.*, 12(3–4), 378–400.
- Pebesma, E. J., and Wesseling, C. G. (1998). "Gstat: A program for geostatistical modelling, prediction and simulation." *Comput. Geosci.*, 24(1), 17–31.
- Przybysz-Jarnut, J. K., Hanea, R. G., Jansen, J. D., and Heemink, A. W. (2007). "Application of the representer method for parameter estimation in numerical reservoir models." *Comput. Geosci.*, 11(1), 73–85.
- Sanchez-Vila, X., Carrera, J., and Girardi, J. (1996). "Scale effects in transmissivity." *J. Hydrol.*, 183(1), 1–22.
- Stauffer, F., Attinger, S., Zimmermann, S., and Kinzelbach, W. (2000). "Uncertainty estimation of well catchments in heterogeneous aquifers." *Water Resour. Res.*, 38(11), 1238.
- Sun, N.-Z., and Yeh, W. W.-G. (1985). "Identification of parameter structure in groundwater inverse problem." *Water Resour. Res.*, 21(6), 869–883.
- Vrugt, J. A., Stauffer, P. H., Wohling, T., Robinson, B. A., and Vesselinov, V. V. (2008). "Inverse modeling of subsurface flow and transport properties: A review with new developments." *Vadose Zone J.*, 7(2), 843–864.
- Yeh, T. C. J., Jin, M., and Hanna, S. (1996). "An iterative stochastic inverse method: Conditional effective transmissivity and hydraulic head fields." *Water Resour. Res.*, 32(1), 85–92.
- Zhang, Y. (2014). "Nonlinear inversion of an unconfined aquifer: Simultaneous estimation of heterogeneous hydraulic conductivities, recharge rates, and boundary conditions." *Transp. Porous Media*, 102(2), 275–299.
- Zhang, Y., Irsa, J., and Jiao, J. Y. (2014). "Three-dimensional aquifer inversion under unknown boundary conditions." *J. Hydrol.*, 509, 416–429.
- Zhang, Y., Person, M., and Gable, C. W. (2007). "Representative hydraulic conductivity of hydrogeologic units: Insights from an experimental stratigraphy." *J. Hydrol.*, 339(1–2), 65–78.
- Zheng, C. (2010). "MT3DMS v5.3 supplemental user's guide." *Technical Rep.*, U.S. Army Engineer Research and Development Center, Dept. of Geological Sciences, Univ. of Alabama, Tuscaloosa, AL.
- Zlotnik, V. A., Zurbuchen, B. R., Ptak, T., and Teutsch, G. (2000). "Support volume and scale effect in hydraulic conductivity: Experimental aspects." *Theory, modeling, and field investigation in hydrogeology: A special volume in honor of Shlomo P. Neuman's 60th birthday*, D. Zhang and C. L. Winter, eds., Geological Society of America, Boulder, CO, 215–231.